Transportation Engineering 2 (2020) 100017

Contents lists available at ScienceDirect

Transportation Engineering

journal homepage: www.elsevier.com/locate/treng

# A multilevel finite element-multibody approach to design the suspension system for the road transportation of SSR1 cryomodule

P. Neri [a,*], F. Bucchi [a], D. Passarelli [b]

[a] DICI – Department of Civil and Industrial Engineering, University of Pisa, Largo L. Lazzarino 2, Pisa 56122, Italy
[b] Fermilab, Batavia, IL, USA

ARTICLE INFO

*Keywords:*
Suspension system
Cryomodule transportation
Vibration isolation
Reduced order modeling
Mechanical filter

ABSTRACT

Cryomodules (CM) represents edge-frontier assemblies in particle physics research field. The road transportation of CM is a critical phase during which the structures can be subjected to significant dynamic loads. It is therefore necessary to design a Transportation Tool (TT) equipped with an appropriate suspension system. This work describes the approach adopted for the design of the TT for the CM PIP-II SSR1 (Proton Improvement Plan-II – Single Spoke Resonators 1), which is firstly introduced in the CM research field. Initially a Finite Element (FE) model was developed, considering the main sub-assemblies of the CM. However, this model was not suitable for the design of the TT due to the high computational burden. For this reason the model was exported as a Modal Neutral File and imported into a MultiBody software (MB) where the remaining components were modeled as concentrated stiffnesses or rigid bodies. The MB model thus obtained has drastically reduced the calculation time, proving to be fundamental in the TT iterative design phase, which involves the use of Helical Isolators (HI) performing the function of mechanical filters. To validate the effectiveness of TT in reducing dynamic loads, a 3D acceleration profile measured during the transport of a similar cryomodule (Linear Coherent Light Source II, LCLS-II) was used. Furthermore, the results of the MB model were used to perform the structural verification of some critical components of the CM.

## 1. Introduction

The PIP-II (Proton Improvement Plan-II) project conducted at Fermilab is a proton driver superconducting linac consisting of five different types of Superconducting Radio Frequency (SRF) cavities [1]: half wave resonator (HWR) [2,3], 325 MHz single spoke resonators (SSR1, SSR2) [4], and 650 MHz multicell cavities (LB650, HB650) [5], which exploits superconducting materials [6] to accelerate the particles beam in a vacuum environment [7]. A fundamental step in the design of these devices is determined by the development of supports and procedures suitable for mitigating damage during the transport phase [8,9]. The prototype of the cryomodule (CM) SSR1 is currently being assembled at Fermilab and will be subject to numerous journeys by truck between different facilities of the research center. The speed of the truck will be limited to around 10 m/s. The design of a transport system suitable for the safe handling of the cryomodule is then mandatory and it is the topic of a collaboration between the Department of Civil and Industrial Engineering of the University of Pisa and the Technical Division of the Fermi National Accelerator Laboratory (Fermilab, Batavia, IL). This activity is typically carried out basing on previous experiences or on approximate analyses. Therefore, the purpose of this activity was to establish a rigorous design procedure that would allow both the correct dimensioning of the Transportation Tool (TT) and the evaluation of the performance in terms of suppression of dynamic loads during the simulation phase.

In the literature, many papers deal with vibration: indeed, several papers deal with the analysis of the driver and passenger comfort in different type of vehicles and are aimed at reducing the seat vibration through optimized [10] active or semi–active suspensions [11–13] or through the introduction of additional elements like inerters [14]. Concerning transported freights, many papers [15–18] deal with the qualitative analysis of damage during transportation of fragile elements (e.g. fruit or vegetables) or measure the on road acceleration of the truck loading bed in different operating conditions [19–21]. Other papers [22–25] describe the development of multi–body models aimed at predicting the acceleration and vibration level of vehicle, passengers and transported freights. Finally, some papers [26,27] deal with the structural analysis of vehicle parts during transportation. To the best of the authors' knowledge, no paper deal with the design of additional structures aimed at reducing the vibration of cryomodule on truck and the quantitative analysis of transportation dynamics and structural stress through dedicated numerical modeling.

* Corresponding author.
*E-mail address:* paolo.neri@dici.unipi.it (P. Neri).

https://doi.org/10.1016/j.treng.2020.100017
Received 23 June 2020; Received in revised form 24 July 2020; Accepted 27 August 2020

**List of symbols**

| Symbol | Description |
|---|---|
| $U_x$ | Unitary displacement along $x$-axis |
| $U_y$ | Unitary displacement along $y$-axis |
| $U_z$ | Unitary displacement along $z$-axis |
| $\vartheta_x$ | Unitary rotation along $x$-axis |
| $\vartheta_y$ | Unitary rotation along $y$-axis |
| $\vartheta_z$ | Unitary rotation along $z$-axis |
| $F_x$ | Reaction force along $x$-axis |
| $F_y$ | Reaction force along $y$-axis |
| $F_z$ | Reaction force along $z$-axis |
| $M_x$ | Reaction moment along $x$-axis |
| $M_y$ | Reaction moment along $y$-axis |
| $M_z$ | Reaction moment along $z$-axis |
| $f^{FE}_{V+TS}$ | Natural field computed through Finite Element analysis of the vessel + thermal shield |
| $f^{MB}_{V+TS}$ | Natural field computed through Multibody analysis of the vessel + thermal shield |
| $f^{MB}_{CM}$ | Natural field computed through Multibody analysis of the entire cryomodule |
| $\delta_{st}$ | Vertical static compression of the suspension |
| $\omega_n$ | Natural frequency of the 1-dof mass-spring model |
| $g$ | Acceleration of gravity |
| $k^{tot}_v$ | Total vertical stiffness of the suspension system |
| $m$ | Sum of the mass of the CM and the TT |
| $\delta_x$ | Displacement along $x$-axis |
| $\delta_y$ | Displacement along $y$-axis |
| $\delta_z$ | Displacement along $z$-axis |
| $k_x$ | Bushing stiffness along $x$-axis |
| $k_y$ | Bushing stiffness $y$-axis |
| $k_z$ | Bushing stiffness $z$-axis |
| $f$ | Mode Frequency |
| $x_{cav}$ | Lateral displacement of the center of mass of the reference cavity |
| $y_{cav}$ | Vertical displacement of the center of mass of the reference cavity |
| $y_{lp}$ | Vertical displacement of the loading bed |
| $y_{lp}$ | Vertical displacement of the loading bed |
| $\sigma^i_{xx}$ | Normal stress acting on the bellow along the $x$-axis |
| $\sigma^i_{yy}$ | Normal stress acting on the bellow along the $y$-axis |
| $\sigma^i_{zz}$ | Normal stress acting on the bellow along the $z$-axis |
| $\tau^i_{xy}$ | $xy$-shear stress |
| $\tau^i_{yz}$ | $yz$-shear stress |
| $\tau^i_{xz}$ | $xz$-shear stress |
| $i$ | Node number |
| $\widetilde{K}^i$ | Nodal equivalent stiffness matrix |
| $\widetilde{K}^i_{ij}$ | $ij$-element of the bellow stiffness matrix |
| $\sigma_{eq,max}$ | Maximum equivalent stress |
| $B_n$ | $n$th bellow |

*List of abbreviations*

| Abbreviation | Description |
|---|---|
| CM | Cryomodule |
| TT | Transportation Tool |
| FE | Finite Element |
| MB | Multi Body |
| HI | Helical Isolator |
| PIP-II SSR1 | Proton Improvement Plan-II – Single Spoke Resonators 1 |
| LCLS-II | Linear Coherent Light Source II |
| SRF | Superconducting Radio Frequency |
| HWR | Half Wave Resonator |
| MNF | Modal Neutral File |
| FRF | Frequency Response Function |
| EJMA | Expansion Joint Manufacturer Association |
| DoF | Degree of Freedom |
| WI/WOI | With/WithOut Isolators |

In this paper, the design of the a transport system is presented. The design started from the study of the dynamic response of the CM using a complete model based on a combination of Finite Element analysis (FE) and Multi Body simulations (MB), using Ansys and MSC Adams software respectively, an approach that has already demonstrated its effectiveness in simulating complex assemblies [25]. Subsequently, it was possible to design the suspension system that acts as a mechanical filter to isolate the CM components from dynamic loading generated by the truck and the road. The main components (considered as deformable) were modeled in the FE environment, and the results were then imported into a complete MB model that also considered minor components, modeled as lumped stiffnesses and masses. This model has much shorter computation times with respect to the full FE model, and can therefore be used in the design phase, evaluating the performance of the TT under the effect of dynamic loads of various kinds. In the first instance, it was possible to evaluate the filtering effect of the TT by measuring the displacements of the various components on the MB model under the effect of certain dynamic loads. Subsequently, the loads determined by the MB model could be used in specific detailed FE models of the critical components to evaluate the stress distribution during transport. Also, a lean and fast calculation method for this last detailed simulation phase was proposed, which drastically reduces the computational burden, allowing to quickly evaluate the effects of complex load histories without the need to repeat the FE simulations for each time instant. It is worth noting that no paper in literature were found applying a similar work-flow to the design of CM transportation tool.

## 2. Finite element analysis

The design of the TT required a preliminary estimation of the dynamic behavior of the CM. Since the TT mainly acts as a mechanical filter with respect to the dynamic load of the road, it was crucial to evaluate the main natural frequencies of the CM in order to identify the required cut-off frequency. This was achieved through a combined FE and MB approach. Firstly, an FE model was developed. Since the entire assembly included thousands of parts, it was necessary to identify the main sub-assemblies, considering their impact on the total mass of the CM and their potential critical behavior during transportation.

### 2.1. FE model

Most of the CM geometries were characterized by a small thickness, therefore mainly shell elements have been used. Shapes, material properties and thicknesses for all the components were obtained from the 3D model and the assembly drawings. For the FE modeling the following parts have been selected (Fig. 1): vessel, thermal shield, strongback, cavities, support posts and solenoids. This preliminary FE model does not take into consideration either the two-phase pipe or the bellows connecting the various parts. In fact, their detailed geometry would require an enormous number of elements to obtain reliable results, resulting in extremely long calculation times. These parts, which can actually be critical during transport, will be taken into consideration in subsequent analysis through MB modeling. Each of the six mentioned subgroups was initially modeled separately for simplicity, and all the sub-assemblies were finally imported into the full assembly to produce the complete model of the CM. All the connections between the parts have been set by node merge and fixed joints, to completely avoid the use of contact elements.

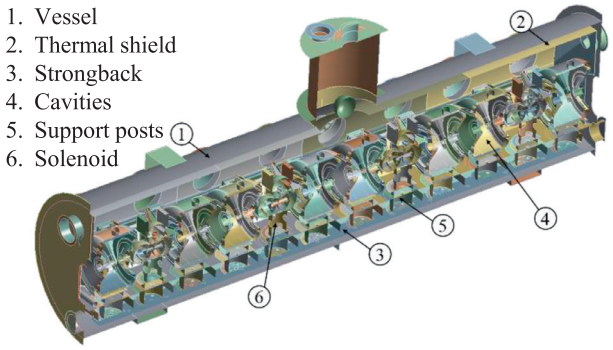


**Fig. 1.** Main subassemblies of the FE model.

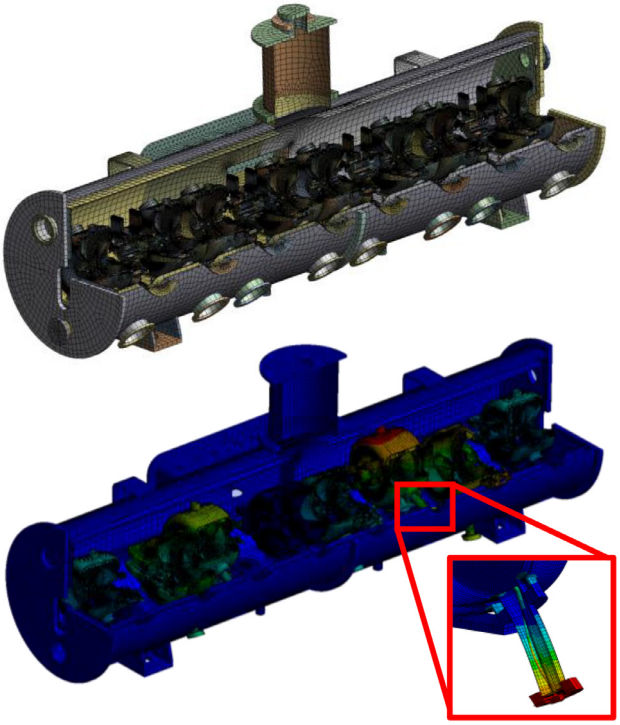

**Fig. 2.** Examples of results for the full model.

The final model has a total mass of about 6200 kg, which is almost 75 % of the total estimated mass of the CM (for computational reasons minor details, i.e. cables, bolts, pipes etc., were not included in the model), with a total number of $1.1 \times 10^6$ nodes and $1.2 \times 10^6$ elements (quadratic order). Modal analysis took about 5 h to calculate the first fifty modes of the CM on a Intel Xeon dual-core workstation X5660, 2.8 GHz, 48 Gb of RAM (up to 85 % used during solution). Fig. 2 shows a section view of the complete model and an example of its natural mode (high frequency).

### 2.2. Bellows FE model

As anticipated, the presented FE model does not take into account potential critical parts, such as the bellows that allow compensation of thermal deformations during operation. These components, however, have been considered in the MB model (see "Multibody Analysis" section) through lumped stiffnesses with six degrees of freedom, defined by a $6 \times 6$ stiffness matrix. Six different bellows with different geometries are used in the CM ($B_n$, $n = 1 \dots 6$). To calculate the value of the coefficients of this matrix, a dedicated FE model has been set for each bellow. The model has been meshed with shell elements, since the

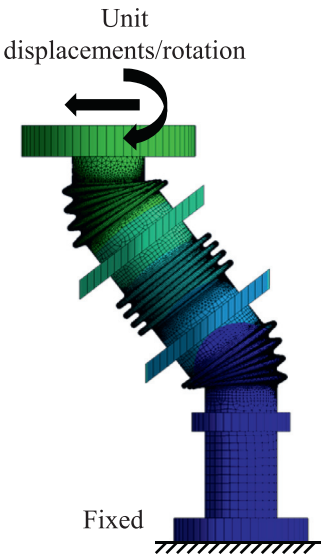


**Fig. 3.** Displacement/constraint scheme of a bellow.

thickness of all the bellows is much lower than their radius. Fig. 3 shows the displacement/constraint scheme applied to the bellow. At one end of the bellow fixed constraint was imposed, while on the other end a unitary displacement was applied along eachone of the six degrees of freedom, i.e. 3 translations ($U_x$, $U_y$, $U_z$) and 3 rotations ($\vartheta_x$, $\vartheta_x$, $\vartheta_z$). The bellow equivalent stiffness matrix was then calculated by measuring the reaction forces ($F_x$, $F_y$, $F_z$) and moments ($M_x$, $M_y$, $M_z$) corresponding to each load condition: each of the six loading conditions defined a column of the stiffness matrix, as follows:

$$\begin{bmatrix} F_x \\ F_y \\ F_z \\ M_x \\ M_y \\ M_z \end{bmatrix} = \begin{bmatrix} & K & \end{bmatrix} \begin{bmatrix} U_x \\ U_y \\ U_z \\ \vartheta_x \\ \vartheta_y \\ \vartheta_z \end{bmatrix} \tag{1}$$

The same model was also used to evaluate the natural frequencies of the bellows themselves, so as to verify that they were significantly higher than the frequency of the mechanical load to which they will be subjected during transport. This verification allowed to consider these elements as concentrated stiffnesses, neglecting their inertial effects during transport simulations.

## 3. Multibody analysis

In order to calculate the eigenfrequencies of the entire cryomodule and, subsequently, to evaluate the filtering effects of the TT, a multibody model was developed. The model, shown in Fig. 4, was composed of various parts, implemented through different modeling strategies:

- The external vessel of the cryomodule, together with the thermal shield, the strongback and the solenoids (n. 1 in Fig. 4) have been exported by the FE software as a modal neutral file (mnf, reduced model), a format that allows to consider the deformability of all structures through the Craig-Bampton modal reduction technique [28]. Using this technique, the degrees of freedom of the model have been reduced from around $8 \times 10^5$ to about 330.
- The two-phase pipe, n. 2, was modeled by dividing the pipe into different beam elements interconnected by forces and moments whose magnitude was determined through the Timoshenko beam theory.
- The cavities, n. 3, were imported as rigid bodies, considering their real properties of mass and inertia. The hypothesis to consider them as rigid bodies was justified by a preliminary FE modal analysis of the

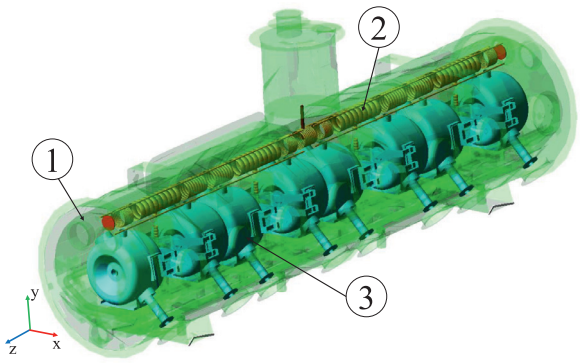


**Fig. 4.** MultiBody model of the full cryomodule.

**Table 1**
Natural frequencies for FE and MB models.

| Mode # | $f^{FE}_{V+TS}$ (Hz) | $f^{MB}_{V+TS}$ (Hz) | $f^{MB}_{CM}$ (Hz) |
|---|---|---|---|
| 1 | 9.5 | 9.5 | 9.6 |
| 2 | 15.4 | 15.3 | 15.2 |
| 3 | 17.2 | 17.1 | 17.9 |
| 4 | 19.1 | 18.8 | 21.6 |
| 5 | 21.2 | 20.8 | 23.1 |

cavities themselves, which showed that the first natural frequency (about 150 Hz) was clearly higher than the frequencies of interest during transport: as analyzed in [29], the spatial (cycles/m) excitation frequency due to road roughness is appreciable up to about frequency values of 1.5–2 cycles/m, which corresponds to an excitation frequency of about 15–20 Hz for a vehicle traveling at 10 m/s.

- The bellows, which are not represented in Fig. 4, were modeled as concentrated stiffnesses, whose characteristics (matrix of equivalent stiffness) were obtained by finite element analysis.

At each connection point of the part n. 1 a master node was selected during the FE simulation and it was used to connect this parts to the others. In particular, the cavities were connected using a certain amount of hinge joints to simulate the bolts of the flanged connection, while the two phase pipe was connected to the cavities using bellows. As anticipated in the FE analysis, the bellows were reproduced through equivalent stiffness matrix involving both displacement and rotation degrees of freedom.

### 3.1. MB model validation

In order to verify the accuracy of the imported reduced model, a first modal analysis was performed in the MB environment of the cryomodule vessel together with the thermal shield, strongback and solenoids (this configuration is called Vessel + Thermal Shield, V + TS), imported as deformable bodies, and cavities modeled in the form of rigid bodies. The natural frequencies calculated were compared with those obtained through a complete analysis of the corresponding model using the FE software. Subsequently, the two-phase pipe and bellows were added, and the natural frequencies of the entire cryomodule were calculated in the multibody environment (this configuration is called Cryomodule, CM). Table 1 shows the results of the modal analysis for the FE and MB models. The comparison was carried out up to about 20 Hz because, due to the low speed of the truck, the amplitude of the vibrations related to the roughness of the road at higher frequency was considered negligible.

Concerning the modal reduction procedure, the comparison between $f^{FE}_{V+TS}$ and $f^{MB}_{V+TS}$ confirms the accuracy of the reduction and import technique: the differences in terms of natural frequency of the first five natural modes never exceed 2 %. Furthermore, a check of the modal shapes was also carried out, supporting the correspondence between the two models. The natural frequencies of the complete model listed in Table 1 ($f^{MB}_{CM}$) were close to those computed for the sole imported parts through the *mnf* model ($f^{MB}_{V+TS}$), since the difference in terms of frequency of the first five modes is always less than 15 %. A slight variation of the modal shapes was found, compared to the V + TS analysis, due to the contribution of the mass and inertia of the rigid cavities. However, the addition of the two-phase pipe, the bellows and the cavities does not introduce new low-frequency modes that could be dangerous during transport. Fig. 5 shows the modal shapes associated with the first and second natural modes. The first natural mode involves the oscillation of the thermal shield along the longitudinal axis (z), the other parts of the CM being almost stationary. This mode was not considered particularly critical as it does not include significant deformations of the bellows, which are the most critical components of the CM. On the contrary, the second natural mode is related to the lateral bending of the two-phase pipe and of the cavities and involves a relevant deformation of the bellows. For this reason, this mode is considered the most critical in the low frequency range.

## 4. Suspension system design

A first estimate of the stiffness of the suspension system was performed considering only the heave of the cryomodule: to this aim the mass of the CM was assumed to be vertically supported by the elasticity of the helical isolator system, and the 1-dof model was used to asses the first natural mode. The stiffness of the suspension system influences both the vertical travel of the CM and the mechanical filtering effect. In particular, the greater the stiffness, the lower the travel and the effectiveness of the filter. Considering as a target a vertical static compression of the suspension $\delta_{st} = 25$ mm, determined basing on the layout constraints, the natural frequency of the CM heave mode together with the TT was calculated as follows:

$$f_{Heave} = \frac{1}{2\pi}\omega_n = \frac{1}{2\pi}\sqrt{\frac{g}{\delta_{st}}} = 3.1 \text{ Hz} \tag{2}$$

where $\omega_n$ is the natural frequency of the 1-dof mass-spring model and $g$ is the acceleration of gravity. Being sufficiently lower than the natural frequency of the first and second natural modes calculated in the previous section, the mechanical filtering effect of this first attempt configuration should be appreciable. The total vertical stiffness $k_v^{tot}$ of the suspension system required to obtain the frequency was obtained based on the following expression:

$$k_v^{tot} = 4m\pi^2 f^2_{Heave} = 3600 \text{ N/mm} \tag{3}$$

where $m$ is the sum of the mass of the CM and the TT. This first attempt value allowed to identify the order of magnitude of the stiffness of the needed springs and, therefore, a plausible family of commercial products. Basing on this information, the draft of the TT shown in Fig. 6 was designed.

The TT consists of an external frame, rigidly fixed to the truck loading bed, and an internal frame, flanged to the supports of the CM. Internal and external frame are connected by 12 helical isolators (HI) [30], whose characteristics have been selected starting from the first estimation of vertical stiffness [31]. The linearized characteristics of the HIs have been implemented in the MB environment through the bushing element that calculates the force along the three directions ($F_x$, $F_y$, $F_z$) starting from the displacement along the same degrees of freedom ($\delta_x$, $\delta_y$, $\delta_z$):

$$\begin{bmatrix} F_x \\ F_y \\ F_z \end{bmatrix} = \begin{bmatrix} k_x & 0 & 0 \\ 0 & k_y & 0 \\ 0 & 0 & k_z \end{bmatrix} \begin{bmatrix} \delta_x \\ \delta_y \\ \delta_z \end{bmatrix} \tag{4}$$

where $k_x$, $k_y$ and $k_z$ are the stiffnesses of the bushings along the three directions. The frequencies related to the natural modes of the rigid system of the CM mounted on the TT were calculated in the multibody environment, and are shown in Table 2.

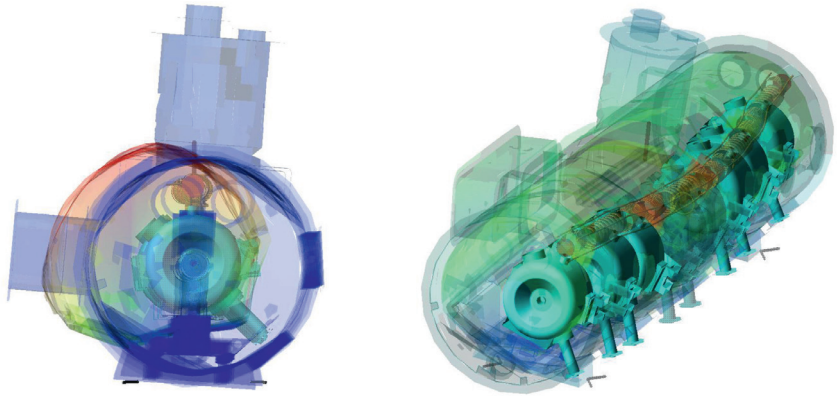

(a) First Natural Mode (b) Second Natural Mode

**Fig. 5.** Deformed shape for first and second natural modes.

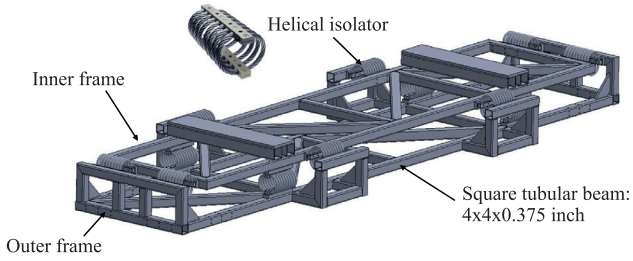


**Fig. 6.** Transportation Tool design with helical isolators.

**Table 2**
Natural frequencies of the system CM + TT.

| Mode # | Description | $f$ (Hz) |
|---|---|---|
| 1 | Roll | 1.9 |
| 2 | Pitch | 3.0 |
| 3 | Heave | 3.3 |
| 4 | Yaw | 4.1 |
| 5 | Mixed 1 | 4.5 |
| 6 | Mixed 2 | 5.3 |

The first four modal shapes were simpler and could be directly correlated to the conventional shapes found in common vehicles. Concerning the fifth and sixth modes, instead, the modal shapes were more complex and not uniquely classifiable in a concise manner. The six natural frequencies were within the range 1.9–5.3 Hz, sufficiently lower than the first and second modes of the CM considered as a deformable body. It has also been verified that the first and the second natural modes of the CM considered as a deformable body do not change significantly due to the introduction of TT and HI. In order to quantitatively assess the mechanical filtering effect of the TT including HI, a harmonic response analysis was performed, imposing three different unitary inputs to the truck's loading bed: heave, roll and pitch. For each input, the vertical displacement ($y$ axis) and lateral ($x$ axis) of the center of mass of one of the cavities were measured and plotted as a frequency response function (FRF), normalized with respect to the intensity of the applied force. For brevity, only the results related to the heave input are presented. Figs. 7 and 8 show, respectively, the FRF of the vertical and lateral displacement of the center of mass of the reference cavity ($y_{cav}$ and $x_{cav}$, respectively), normalized with respect to the amplitude of the vertical heave input (i.e. loading bed, $y_{lp}$), both obtained with and without helical isolators. Considering the vertical displacement ($y$) of the cavity, a low frequency amplification of about 2.5 times was observed (for $f \simeq 3$ Hz), due to the resonance of the heave mode. However, this is not critical since no deformable mode is affected by this frequency. This means that

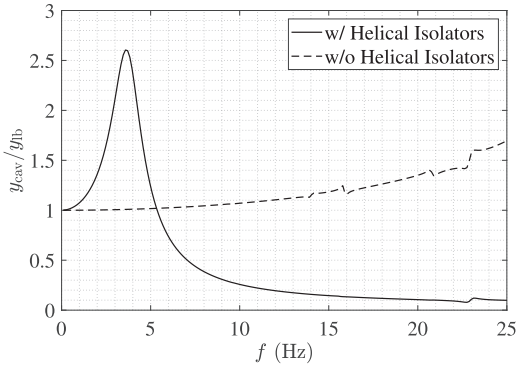


**Fig. 7.** FRF of the vertical displacement: with and without the HI.

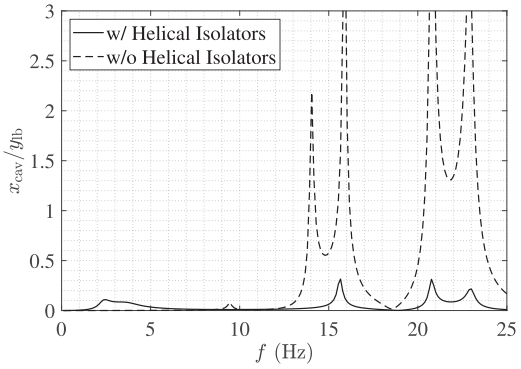


**Fig. 8.** FRF of the lateral displacement: with and without the HI.

the response is characterized by a rigid motion of the CM. For higher frequency values (i.e. $f > 5$ Hz) the response in the vertical direction is reduced (amplitude $< 1$ in Figure 7) thanks to the effect of the mechanical filter. In particular, considering the frequency values corresponding to the first and second natural frequencies of the CM, the vertical input was reduced by a factor of 4 and 5 respectively. Considering the lateral displacement ($x_{cav}$) of the reference cavity, Fig. 8, high values were found in the case of the TT configuration without springs, due to the resonance of the second natural mode. This effect could be critical for the bellows from the structural point of view. However, if HI (solid lines in Figs. 7 and 8) are used, the lateral displacement is greatly reduced. Similar considerations can be inferred for higher frequency modes and for pitch and roll inputs.

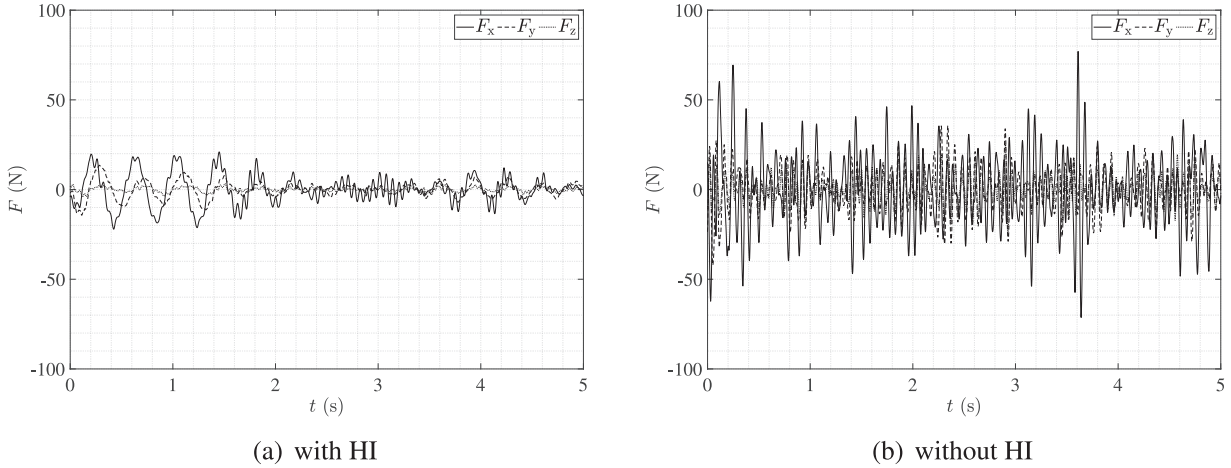


**Fig. 9.** Forces acting on a reference bellow.

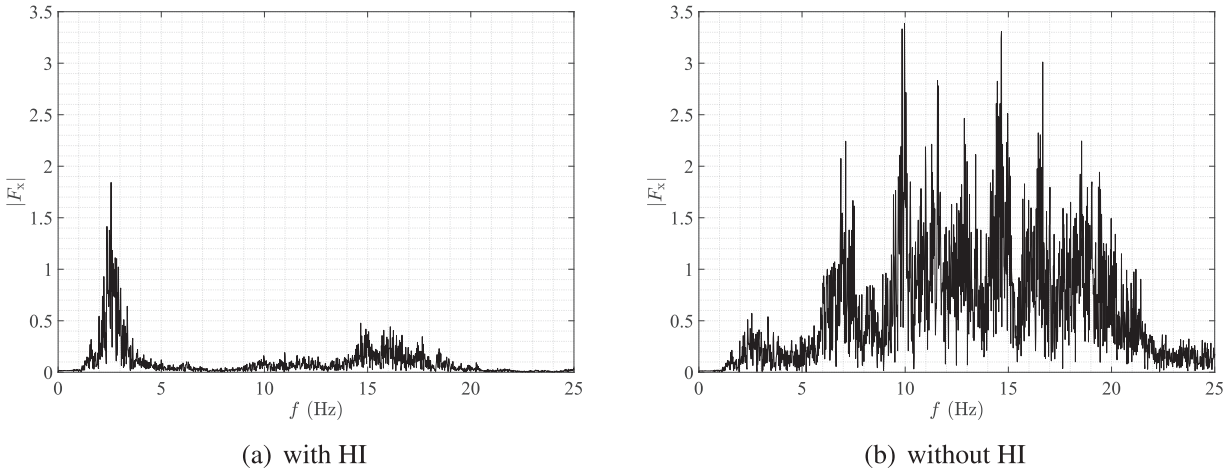


**Fig. 10.** FFT of the Forces acting on a reference bellow (*x* direction).

## 5. Simulation of transportation

To evaluate the loads acting on the CM components during transport with or without HIs, a dynamic transient simulation was performed in the MB environment. The 3D displacement time history of the truck loading bed was imported into the model from the data recorded during the transportation of a CM similar to SSR1. A one-minute reference acquisition was considered, within which the maximum displacement value measured during transport was contained. The forces acting on each component were then recorded during the simulations, paying particular attention to the forces acting on the bellows. Fig. 9 shows the components *x, y* and *z* of the force acting on a reference bellow, in the case of TT equipped with HI (Fig. 9(a)) and TT without HI (Fig. 9(b)). For the considered bellow, each force component never exceeded 25 N if HI isolatos were used, while it was close to 75 N if rigid connection was considered. Than, using HI, a relevant reduction in the amplitude of forces is appreciable, due to the effect of mechanical filtering. In particular, if we consider the spectral analysis of the force acting on the reference bellow (only the component *x* is presented for brevity, as the results along the other directions are similar), the filtering effect can be directly appreciated. In fact, as shown in Fig. 10, considering the layout of the rigid TT (Fig. 10(b)), the force contribution associated with frequencies in the range 10–20 Hz is much higher than in the case where HI are used (Fig. 10(a)). This result testifies that if HI are not used the acceleration coming from the loading bed appreciably excite the natural frequencies of the internal components of the CM which, in many cases, are in the 10–20 Hz range.

## 6. Components structural verification

The proposed modeling approach demonstrated to be highly effective in the estimation of the global dynamic response of the cryomodule. Anyway, the results can also be used for detailed structural verification of critical components. In fact, it was possible to extract displacement information at relevant locations to assess the structural response of any part under the simulated dynamic loading. Indeed, by the knowledge of the relative displacement between e.g. the two ends of a bellow, it is possible to compute through FE analysis the stress acting on it. In this work, two examples are given of this procedure: the RF-antenna response and the bellows structural verification. Both these components are critical from the structural point of view, while their integrity is crucial for the cryomodule operation.

### 6.1. RF-antenna response assessment

The RF-antenna is the slender component represented in Fig. 11, which is used to measure the radio-frequency performance of the cavities during operation. It can be represented as a cantilever beam composed by an external copper tube and an internal steel reinforcement rod. A copper mass is present at the antenna tip, connecting its inner

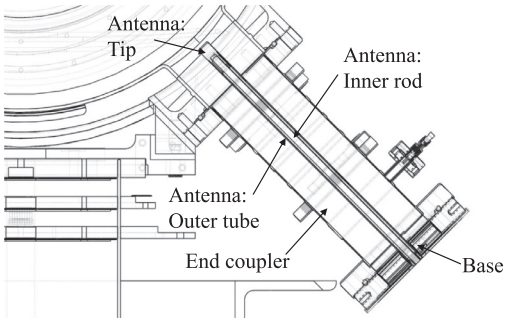


**Fig. 11.** Cross section of RF antenna.

and outer part. The fixed joint of the antenna with the end coupler is obtained through a brazing connection between a steel flange and a ceramic disk.

Due to the slender geometry of the antenna (length 290 mm, diameter 12.7 mm), its tip can be subject to high displacements during transportation, which can cause a brazing failure. Thus, the developed MB model can be used to extract the displacement over time of the antenna tip (with respect to its base) and to compare its amplitude in the case of different suspension solutions. In this work, this task was performed by comparing three different configurations. Firstly, the worst case scenario was considered, i.e. the complete antenna geometry (inner rod and outer tube) in the case of rigid connection between the cryomodule and the truck loading bed. Secondly, the same geometrical configuration was simulated in the case of soft spring mounted on the TT. Finally, the antenna inner rod was removed from the analysis and the antenna behavior was simulated (TT with soft springs). This latter analysis was performed to asses the effect of the inner rod during transportation. The results in Fig. 12 shows the displacement over time of the tip in the plane normal to the antenna axis. This result allows to obtain information about the bending of the antenna. The comparison between Fig. 12(a) and (b) demonstrates that adding the HI to the TT strongly decreases the displacement of the tip, from about 28 μm to about 6 μm. The reduction of the displacement obviously reduces the stress state of the part. On the other hand, the comparison between Fig. 12(b) and (c) highlights that, removing the internal rod, the tip amplitude decreases. Indeed, the internal rod is a useful reinforcement for static forces applied to the antenna tip. On the other hand, it increases the dynamic loading applied to the antenna during transportation, since a relevant amount of mass is added in a region which minimally participate to the antenna bending stiffness.

### 6.2. Bellows structural verification

As already stated, the bellows represent the critical components of the cryomodule. It is then crucial to estimate their response due to dynamic loading, in order to assess if the designed TT performance is sufficient to preserve these components during transportation. A first assessment can be obtained by looking at the displacements of the elements

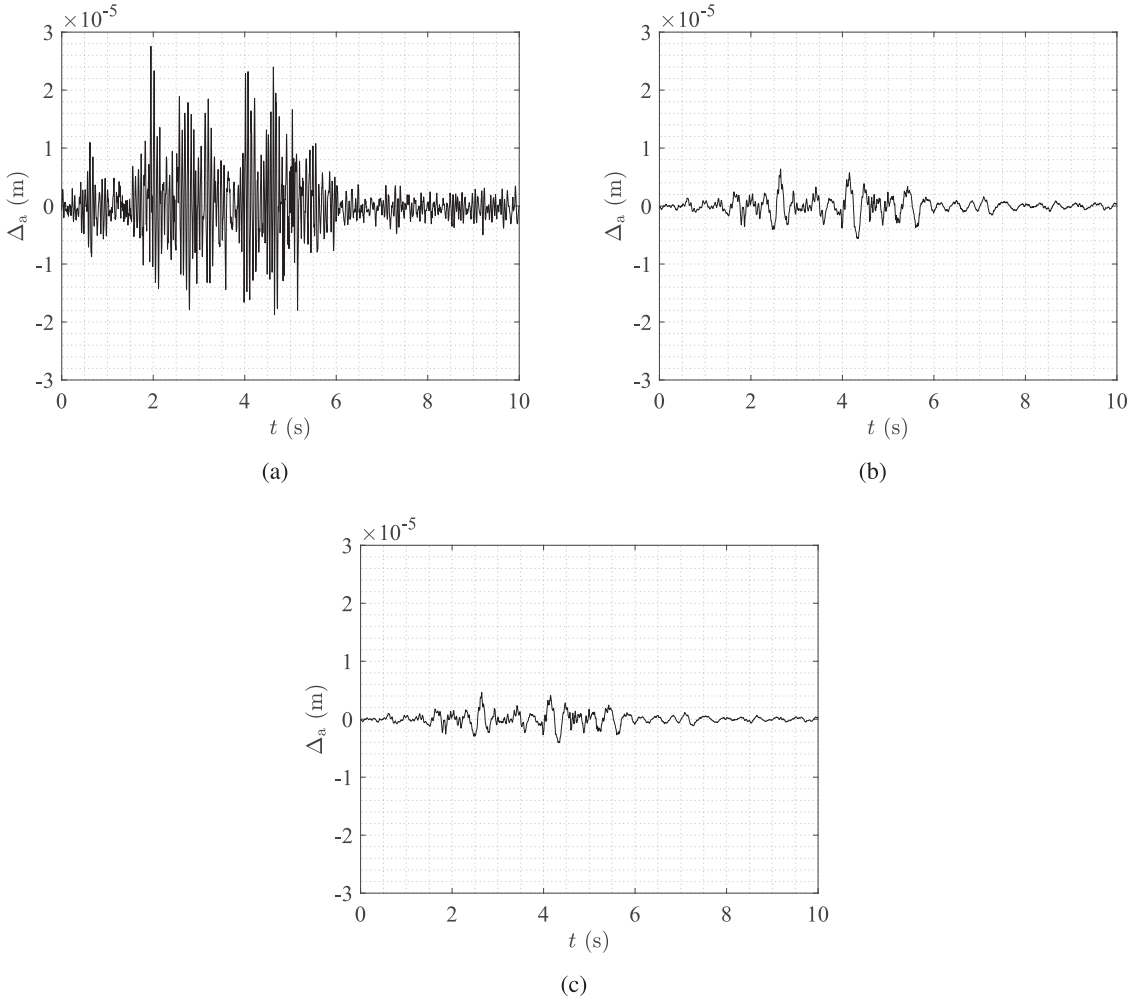


**Fig. 12.** RF antenna displacement: (a) without helical isolators, (b) with helical isolators and (c) with helical isolators after removing the inner rod.

which reproduce the bellows in the model (*field* elements, 6 DoF): the comparison of different solutions (both in time and in frequency domains) can provide valuable information about the filtering effect of the TT, and the displacement amplitudes can be compared to commonly used verification criteria, such as EJMA code (Expansion Joint Manufacturer Association [32]). Otherwise, the displacement amplitude could be used as a load in a dedicated FE model of each bellow. Anyway, the standard verification procedures generally do not take into account a 6 DoF displacement. Also, it is not trivial to assess the worst load combination over time, since the 6 DoF are combined in different ways and it is not possible to assess in advance which is the most critical time instant (i.e. the worst load combination). Thus, the direct verification through EJMA code and FE analysis is cumbersome and highly time consuming. Anyway, it is possible to exploit the linearity of the problem to speed up the computation. Indeed, the stresses acting on the bellow (both normal, i.e. $\sigma^i_{xx}$, $\sigma^i_{yy}$, $\sigma^i_{zz}$ and shear $\tau^i_{xy}$, $\tau^i_{yz}$, $\tau^i_{xz}$) due to any load combination can be computed as a linear combination of the stresses caused by unitary loading along each possible DoF, as expressed in Eq. (5) for the *i*th node.

$$\begin{bmatrix}\sigma^i_{xx}\\ \sigma^i_{yy}\\ \sigma^i_{zz}\\ \tau^i_{xy}\\ \tau^i_{yz}\\ \tau^i_{xz}\end{bmatrix} = \begin{bmatrix}\widetilde{K}^i_{11} & \widetilde{K}^i_{12} & \widetilde{K}^i_{13} & \widetilde{K}^i_{14} & \widetilde{K}^i_{15} & \widetilde{K}^i_{16}\\ \widetilde{K}^i_{21} & \widetilde{K}^i_{22} & \widetilde{K}^i_{23} & \widetilde{K}^i_{24} & \widetilde{K}^i_{25} & \widetilde{K}^i_{26}\\ \widetilde{K}^i_{31} & \widetilde{K}^i_{32} & \widetilde{K}^i_{33} & \widetilde{K}^i_{34} & \widetilde{K}^i_{35} & \widetilde{K}^i_{36}\\ \widetilde{K}^i_{41} & \widetilde{K}^i_{42} & \widetilde{K}^i_{43} & \widetilde{K}^i_{44} & \widetilde{K}^i_{45} & \widetilde{K}^i_{46}\\ \widetilde{K}^i_{51} & \widetilde{K}^i_{52} & \widetilde{K}^i_{53} & \widetilde{K}^i_{54} & \widetilde{K}^i_{55} & \widetilde{K}^i_{56}\\ \widetilde{K}^i_{61} & \widetilde{K}^i_{62} & \widetilde{K}^i_{63} & \widetilde{K}^i_{64} & \widetilde{K}^i_{65} & \widetilde{K}^i_{66}\end{bmatrix}\begin{bmatrix}U_x\\ U_y\\ U_z\\ \vartheta_x\\ \vartheta_y\\ \vartheta_z\end{bmatrix} \quad (5)$$

Thus, instead of repeating the FE simulation for each time instant (and the corresponding load combination), only six simulations were performed as described in Section Bellows FE model (for the lumped stiffness computation) to compute the matrix $\widetilde{K}^i$ at each node of the model. One end of the bellow was constrained as fixed, and a unit displacement (or rotation) along each DoF was subsequently applied to the other end. It is worth noting that the constraint reactions at both ends of the bellow are equal (except the sign), to fulfill static equilibrium. The six components of the stress vector corresponding to each unitary load were then extracted for each node of the bellow to fill a column of $\widetilde{K}^i$. All the measured $\widetilde{K}^i$ can then be assembled in the comprehensive matrix $\widetilde{K}$ which is a $6N \times N$ matrix ($N$ is the total number of nodes of the FE model. Thus, at each time instant it is sufficient to multiply $\widetilde{K}$ by the $6 \times 1$ vector of generalized displacement to obtain the stresses acting on the bellow at each node and at the considered time instant. This procedure is much faster then the complete FE computation, resulting in a considerable reduction of computational time. The von Mises equivalent stress can be finally computed at each time instant for each node to assess which is the critical location at each time instant and which is the maximum stress in the whole time history. An example of this procedure is represented in Fig. 13 for a sample bellow. A qualitative overview of ten seconds of the displacement time history applied to the bellow along the three directions is shown in Fig. 13(a), demonstrating that the load combination is not trivial nor constant over time. The von Mises stress distribution map in the bellow, at a sample time, is shown in Fig. 13(b), demonstrating the possibility to highlight the critical location at each time instant. Finally, the quantitative representation of the von Mises stress over time for the whole time history is reported in Fig. 13(c).

The described procedure was repeated for all the bellows, allowing to compare different TT solution during design phase, simulating the effect on the bellows in the matter of few hours. The results obtained for the final TT design, for all the bellows, are reported in Table 3, showing the comparison between the maximum equivalent stress ($\sigma_{eq,max}$) obtained with the chosen isolators and in the case of rigid connection between the CM and the truck loading bed (last column reports the ratio between the previous two). The table emphasizes how the introduction of the suspension system allowed to reduce the stresses acting on the bellows of a factor between 3.9 and 5.4, leading to a much safer and bearable stress distribution.

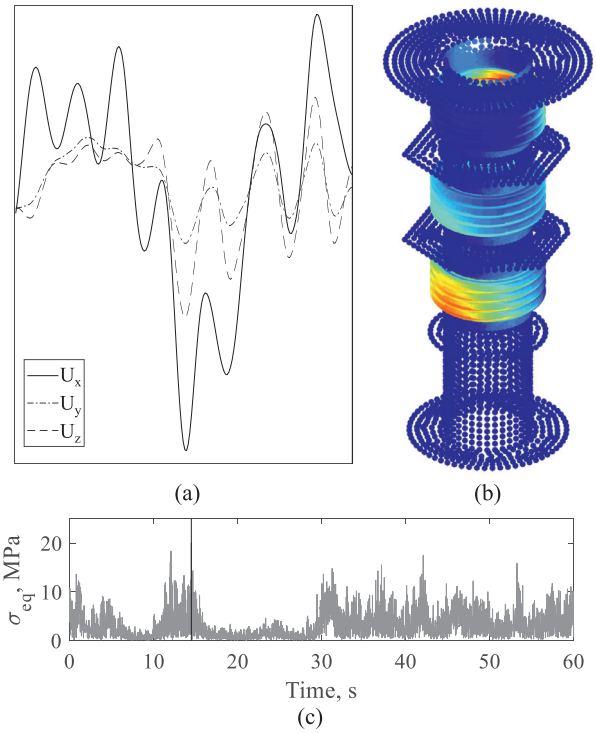


**Fig. 13.** Stresses computation on a sample bellow: (a) few seconds of the applied displacement time history, (b) von Mises stress distribution map at a sample time and (c) equivalent stress in the peak location over time.

**Table 3**
von Mises equivalent stress for the most critical bellow of each kind.

| Bellow | WI, $\sigma_{eq}^{max}$ MPa | WOI, $\sigma_{eq}^{max}$ MPa | Ratio |
|---|---|---|---|
| $B_1$ | 22 | 118 | 5.4 |
| $B_2$ | 60 | 296 | 4.9 |
| $B_3$ | 62 | 282 | 4.5 |
| $B_4$ | 2 | 10 | 5.0 |
| $B_5$ | 29 | 150 | 4.9 |
| $B_6$ | 35 | 137 | 3.9 |

## 7. Conclusions

The described activity allowed to design a reliable Transportation Tool for the SSR1 Cryomodule able to reduce its vibration during transportation. The design phase was structured using a multi-level approach. First of all, a finite element model was developed, including the main subgroups, to evaluate the first natural frequencies of the system. This preliminary analysis provided a rough estimation of the natural frequencies of the transported system and, consequently, of the cut-off frequency required for the Transportation Tool. The results of the FE model were then imported using a reduction technique within a Multi-Body model, in which the missing components were inserted as rigid parts, beams and lumped stiffnesses. This model allowed to carry out a preliminary design of the suspension system, in terms of positioning and stiffness of the springs. These guidelines have been used to select commercial helical isolators and to define the frame geometry.

The effectiveness of the designed TT was evaluated by importing a displacement time history of the truck loading bed measured during the transportation of a CM similar to SSR1. This analysis allowed to evaluate the filtering effect of the TT and to estimate the loads acting on the critical components (such as RF and bellows antennas). These data were used as input of a matrix calculation scheme that allowed to estimate the stresses, and consequently to have information about

the durability of the system, acting on the critical components during transport, highlighting a stress reduction factor of about 4 due to the TT. This analysis, simple but effective, further highlighted the potential of the proposed multi-level approach, which allows both to evaluate the global acceleration response of the system and to quantitatively assess the structural stress of critical components within the same simulation environment. The described activity, which was completely numerical in this phase, must be validated through an experimental campaign. After a phase of experimental modal analysis, aimed at validating the main hypotheses underlying the models, the quality of the proposed design procedure will be evaluated through a trial transportation of the CM between two plants at Fermilab, similarly to the study presented in [33]. The reliability of the models will be quantified through the use of numerous accelerometers positioned in critical points of the structure, such as the cavities and the strongback.

## Declaration of Competing Interest

The authors declare that they have no known competing financial interests or personal relationships that could have appeared to influence the work reported in this paper.

## Acknowledgments

The authors are grateful to the University of Pisa for supporting this research activity (Grant PRA_2018_80).

## References

[1] G. Wu, SRF cryomodules for pip–2 at fermilab, in: Proceedings of the Nineteenth International Conference RF Superconductivity SRF 19, 2019, p. Germany.
[2] Z. Conway, A. Barcikowski, G. Cherry, R. Fischer, B. Guilfoyle, C. Hopper, M. Kedzie, M. Kelly, S. Kim, S. MacDonald, P. Ostroumov, T. Reid, V. Lebedev, A. Lunin, Progress towards a 2.0 k half-wave resonator cryomodule for fermilabs pip-ii project, in: Proceedings of the Twenty-eighth Linear Accelerator Conference, LINAC 2016, 2016.
[3] S. Kim, Z. Conway, M. Kelly, P. Ostroumov, S. Gerbick, T. Reid, M. Kedzie, S. MacDonald, D. Caldwell, Preservation of quality factor of half wave resonator during quenching in the presence of solenoid field, in: Proceedings of the Sixth International Particle Accelerator Conference, IPAC 2015, 2015.
[4] D. Passarelli, R. Wands, M. Merio, L. Ristori, Methodology for the structural design of single spoke accelerating cavities at fermilab, Nucl. Instrum. Methods Phys. Res. Sect. A: Accel. Spectrom. Detect. Assoc. Equip. 834 (2016) 1–9.
[5] J.L. amd E.R. Harms Jr., A. Hocker, T. Khabiboulline, N. Solyak, T. Wong, Development and integration testing of a power coupler for a 3.9-ghz superconducting multicell cavity resonator, IEEE Trans. Appl. Supercond. 21 (2011) 21–26.
[6] E. Barzi, G. Gallo, P. Neri, Fem analysis of nb-sn rutherford-type cables, IEEE Trans. Appl. Supercond. 22 (3) (2012).
[7] V. Roger, S. Cheban, T. Nicol, Y. Orlov, D. Passarelli, P. Vecchiolla, Design update of the SSR1 cryomodule for PIP-II project, in: Proceedings of the Nineth International Particle Accelerator Conference IPAC 18, 2018, p. Canada.
[8] T. Whitlatch, C. Curtis, E. Daly, C. Graves, J. Henry, K. Matsumoto, P. Mutton, J. Pitts, J. Preble, W. Sachleben, W. Schneider, S. Slachtouski, M. Wiseman, Shipping and alignment for the sns cryomodule, in: Proceedings of the 2001 Particle Accelerator Conference, Chicago, 2001.
[9] M. McGee, V. Bocean, C. Grimm, W. Schappert, Transatlantic transport of fermilab 3.9 ghz cryomodule for ttf/flash to desy, in: Proceedings of EPAC08, Genoa, Italy, 2008.
[10] A. Jamali, M. Salehpour, N. Nariman-Zadeh, Robust pareto active suspension design for vehicle vibration model with probabilistic uncertain parameters, Multibody Syst. Dyn. 30 (3) (2013) 265–285.
[11] D. Ning, S. Sun, J. Zhang, H. Du, W. Li, X. Wang, An active seat suspension design for vibration control of heavy-duty vehicles, J. Low Freq. Noise Vib. Act. Control 35 (4) (2016) 264–278.
[12] Y. Wan, J.M. Schimmels, A simple model that captures the essential dynamics of a seated human exposed to whole body vibration, Adv. Bioeng. (1995).
[13] H. Du, W. Li, N. Zhang, Semi-active variable stiffness vibration control of vehicle seat suspension using an mr elastomer isolator, Smart Mater. Struct. 20 (10) (2011) 105003.
[14] Y. Shen, L. Chen, X. Yang, D. Shi, J. Yang, Improved design of dynamic vibration absorber by using the inerter and its application in vehicle suspension, J. Sound Vib. 361 (2016) 148–158.
[15] J. Singh, S.P. Singh, E. Joneson, Measurement and analysis of us truck vibration for leaf spring and air ride suspensions, and development of tests to simulate these conditions, Packag. Technol. Sci.: Int. J. 19 (6) (2006) 309–323.
[16] S. Singh, M. Xu, Bruising in apples as a function of truck vibration and packaging, Appl. Eng. Agric. 9 (5) (1993) 455–460.
[17] B. Jarimopas, S.P. Singh, W. Saengnil, Measurement and analysis of truck transport vibration levels and damage to packaged tangerines during transit, Packag. Technol. Sci.: Int. J. 18 (4) (2005) 179–188.
[18] R. Hinsch, D. Slaughter, W. Craig, J. Thompson, Vibration of fresh fruits and vegetables during refrigerated truck transport, Trans. ASAE 36 (4) (1993) 1039–1042.
[19] A.P. Cann, A.W. Salmoni, T.R. Eger, Predictors of whole-body vibration exposure experienced by highway transport truck operators, Ergonomics 47 (13) (2004) 1432–1453.
[20] F. Lu, Y. Ishikawa, T. Shiina, T. Satake, Analysis of shock and vibration in truck transport in japan, Packag. Technol. Sci.: Int. J. 21 (8) (2008) 479–489.
[21] M.-A. Garcia-Romeu-Martinez, S.P. Singh, V.-A. Cloquell-Ballester, Measurement and analysis of vibration levels for truck transport in spain as a function of payload, suspension and speed, Packag. Technol. Sci.: Int. J. 21 (8) (2008) 439–451.
[22] L. Ventura, G.P. Bonelli, A. Martini, Development and experimental validation of a numerical multibody model for the dynamic analysis of a counterbalance forklift truck, in: Proceedings of thr Fifth Joint International Conference on Multibody System Dynamics, Lisbon, Portugal, 2018.
[23] M. Yang, G. Xu, Q. Dong, X. Han, Vibration study of fork-lift truck based on the virtual prototype technology, Sens. Transduc. 170 (5) (2014) 177–183.
[24] F. Bucchi, F. Frendo, F. Bavaresco, G. Conte, Multibody simulation of a rope-driven automated people mover, Proce. Inst. Mech. Eng. F: J. Rail Rapid Transit 232 (8) (2018) 2173–2185.
[25] L. Bertini, F. Bucchi, B. Monelli, P. Neri, Development of a simplified model for the vibration analysis of lawn mowers, Proc. Struct. Integr. (8) (2018) 509–516.
[26] C. Mi, Z. Gu, Q. Yang, D. Nie, Frame fatigue life assessment of a mining dump truck based on finite element method and multibody dynamic analysis, Eng. Fail. Anal. 23 (2012) 18–26.
[27] S.-H. Lee, T.-W. Park, J.-K. Park, J.-W. Yoon, K.-J. Jun, S.-P. Jung, Fatigue life analysis of wheels on guideway vehicle using multibody dynamics, Int. J. Precis. Eng. Manuf. 10 (5) (2009) 79–84.
[28] R. Craig, M. Bampton, Coupling of substructures for dynamic analysis, AIAA J. (6) (1968) 7.
[29] T.D. Gillespie, Fundamentals of Vehicle Dynamics, 400, Society of automotive engineers Warrendale, PA, 1992.
[30] M. McGee, T. Arkan, E. Borissov, J. Leibfritz, W. Schappert, S. Barbanotti, Transport of desy 1.3 ghz cryomodule at fermilab, in: Proceedings of PAC09, Vancouver, BC, Canada, 2009.
[31] Isolation dynamic corps, http://www.isolator.com/NewDocs/MSeries/M32CurveData.pdf.
[32] The expansion joint manufacturer association, ejma standards. www.ejma.org.
[33] S. Barbanotti, A. Bosotti, M. Fusetti, P. Michelato, A. Bertolini, S. Berry, M. Dorlot, C. Madec, O. Napoly, CEA-Saclay, R. Amirikas, M. Boehnert, C. Engling, D. Hoppe, K. Jensch, D. Kostin, C. Mueller, H. Remde, O. Sawlanski, J. Wojtkiewicz, M. McGee, Monitoring the flash cryomodule transportation from desy hamburg to cea saclay: coupler contact, vacuum, acceleration and vibration analysis, in: Proceedings of PAC09, Vancouver, BC, Canada, 2009.